Journal Pre-proofs

Full-length Article

Early rebalancing of neuroinflammatory cascades lastingly rescues prefrontal deficits in a 22q11.2ds model

Anne Günther, Mattia Chini, Sebastian H. Bitzenhofer, Annette Marquardt, Ileana L. Hanganu-Opatz

PII: S0889-1591(26)00218-7
DOI: https://doi.org/10.1016/j.bbi.2026.106470
Reference: YBRBI 106470

To appear in: *Brain, Behavior, and Immunity*

Received Date: 14 August 2025
Revised Date: 29 December 2025
Accepted Date: 25 January 2026

Please cite this article as: Günther, A., Chini, M., Bitzenhofer, S.H., Marquardt, A., Hanganu-Opatz, I.L., Early rebalancing of neuroinflammatory cascades lastingly rescues prefrontal deficits in a 22q11.2ds model, *Brain, Behavior, and Immunity* (2026), doi: https://doi.org/10.1016/j.bbi.2026.106470

Early rebalancing of neuroinflammatory cascades lastingly rescues prefrontal deficits in a 22q11.2ds model

Anne Günther [1*], Mattia Chini [1], Sebastian H. Bitzenhofer [1,2], Annette Marquardt [1], Ileana L. Hanganu-Opatz [1*]

[1] Institute of Developmental Neurosciences, Center for Molecular Neurobiology, Hamburg Center of Neuroscience, University Medical Center Hamburg-Eppendorf, Hamburg 20251, Germany

[2] Neural Circuit Physiology, Center for Molecular Neurobiology, University Medical Center Hamburg-Eppendorf, 20251 Hamburg, Germany

[*] Corresponding authors: Anne Günther

anne.guenther@zmnh.uni-hamburg.de

Ileana L. Hanganu-Opatz

hangop@zmnh.uni-hamburg.de

Keywords

Prefrontal cortex, development, neuroinflammation, 22q11.2 microdeletion, minocycline, microglia, set-shifting

Running title

Developmental neuroinflammation in a 22q11.2ds model

Abstract

Cognitive deficits, a characteristic feature of neuropsychiatric disorders, reflect perturbed activity in neuronal networks. Increasing evidence has linked neuroinflammation to impaired neuronal activity and resulting cognitive dysfunction, yet the underlying cellular mechanisms

and developmental dynamics remain largely unclear. Here, we address this knowledge gap by investigating the *Df(16)A* mouse model of human 22q11.2 microdeletions, a prevalent chromosomal abnormality associated with an increased incidence of neuropsychiatric disorders. During early postnatal development, *Df(16)A*$^{+/-}$ mice show an imbalance of inflammatory signaling markers accompanied by increased microglial density in the superficial layers of the prefrontal cortex. Consequently, spine densities of pyramidal neurons were decreased, resulting in disrupted patterns of prefrontal neuronal activity during development and poor performance in a set-shifting task at juvenile age. Early treatment with minocycline, an anti-inflammatory drug, lastingly rescued these deficits in *Df(16)A*$^{+/-}$ mice, rebalancing signaling cascades and restoring neural activity as well as cognitive performance. These findings identify the early rebalancing of inflammatory signaling cascades as a promising therapeutic strategy for mitigating pathophysiological trajectories associated with the 22q11.2 deletion syndrome.

1. Introduction

Hemizygous microdeletions at the 22q11.2 locus are among the most common chromosomal abnormalities in the population (1). They predominantly occur *de novo*, although heritability has been reported (2). 22q11.2 microdeletions are associated with a broad spectrum of multisystemic pathophysiological features, including increased incidence of neuropsychiatric pathologies such as schizophrenia, autism spectrum disorder, and attention deficit hyperactivity disorder (3–8). This marked complexity and variability of clinical manifestations for the 22q11.2 deletion syndrome (22q11.2ds) has hindered identification of the underlying pathophysiological mechanisms and, ultimately, of potential therapeutic approaches (9).

In recent years, increasing evidence highlighted the contribution of neuroinflammation (10–13) and especially of microglial activity (14,15) to neuropsychiatric disorders. Microglia, the resident macrophages of the brain, continuously monitor their surrounding tissue and react to the presence of signaling molecules by altering their morphology, transcriptional profiles, and cytokine release (16). A major function of microglia is the shaping of synaptic landscapes in the developing brain by pruning synapses in an experience-dependent manner (17,18). While the etiology of 22q11.2ds does not bear an obvious inflammatory component, increased presence of inflammatory markers and complement components, which are involved in specifically tagging synapses for microglia-mediated pruning, has been reported for samples from patients of this syndrome (13,19). Notably, a marked reduction of dendritic spines and dendritic complexity of excitatory neurons, especially in the prefrontal cortex (PFC) (20–27), has been reported in patients and mouse models of several neuropsychiatric disorders. The PFC is a hub of neuronal networks and it is essential for higher-order cognitive functions, which are frequently impaired in neuropsychiatric disorders (28,29). Prefrontal activity and connectivity patterns are disrupted in prodromal patients of schizophrenia (30) as well as in mouse models of neuropsychiatric disorders (20,21,31), long before the onset of symptoms. When compared to other cortical areas, the PFC shows protracted development (32–34) with pyramidal neurons of superficial layers being among the last in the brain to fully mature (35). However, as a consequence of this prolonged high plasticity, time windows of increased vulnerability might also be extended for the PFC. In support of this hypothesis, it has been reported that interfering with prefrontal development during specific time windows of early and late development has long-lasting effects on cognitive abilities, specifically as a result of layer 2/3 (L2/3) pyramidal neuron dysfunction (20,36–40). As of yet, the basis of this apparent link between early prefrontal disruption and symptoms of neuropsychiatric disease, such as cognitive impairments later in life, remains unclear.

Here, we propose that (i) neuroinflammatory processes in the PFC during development are critical pathophysiological features of the 22q11.2ds and (ii) early recovery of imbalanced neuroinflammatory signaling cascades rescues these pathophysiological trajectories. To test these hypotheses, we investigate the *Df(16)A* mouse model, which bears a hemizygous deletion syntenic to the 1.5 Mb critical region of 22q11.2 microdeletions in humans (41,42). This mouse model largely recapitulates the phenotypic characteristics of the human syndrome, including cognitive deficits and altered neuronal network activity (42,43). Previously, we identified time windows of high plasticity and profound reorganization of prefrontal circuitry as well as of high vulnerability during early (*i.e.* postnatal day (P) 8-11) and late (*i.e.* P28-37) development in wildtype mice (20,36,37,40). Therefore, we will focus on these developmental time windows when assessing the effect of neuroinflammation on prefrontal activity. We show increased density of microglia with altered morphology, accompanied by an imbalance of pro-inflammatory and neuroprotective signaling markers in the PFC of *Df(16)A*$^{+/-}$ mice. This observed shift towards neuroinflammation was present throughout development, yet

particularly prominent during the second postnatal week. Specifically, we identify C1q, a component of the classical complement pathway of microglia signaling, as a potential marker for the pathophysiological trajectory in *Df(16)A* mice. Early treatment with minocycline, an anti-inflammatory agent, rescues the observed imbalance as well as the concurrent reduction of dendritic spines on prefrontal L2/3 pyramidal neurons and the disruption of neuronal activity. Most notably, functional rescue induced by early minocycline treatment persists until late development and is accompanied by a recovery of PFC-dependent cognitive performance of adolescent mice.

2. Results

2.1. Early perturbations of innate behaviors in *Df(16)A*$^{+/-}$ mice

While several studies have characterized functional, neuroanatomical, and behavioral deficits of adult *Df(16)A*$^{+/-}$ mice and similar mouse models of neuropsychiatric disorders (22,26,27,42–44), the developmental profiles of these deficits remain largely unknown. To assess whether *Df(16)A*$^{+/-}$ mice show altered developmental trajectories, we first examined a set of early behavioral readouts: developmental milestones (auditory startle reflex, eye opening, vibrissa placement), early reflexes (bar holding, righting reflex), and innate behaviors (ultrasonic vocalizations (USVs)). During neonatal development (P5-12), *Df(16)A*$^{+/-}$ (from here on referred to as Df16)) and wildtype (referred to as Wt) pups showed similar body weight increase (Figure S1A) and early reflexes (Figure S1B,C). Analysis of developmental milestones revealed that solely the auditory startle was significantly delayed in Df16 mice ($p=0.0068$), whereas other features, such as eye opening or vibrissa placement, were comparable for Df16 and Wt mice (Figure S1D-F). Furthermore, we assessed isolation-induced USVs in P5-12 Df16 and Wt mice (Figure 1A-D, Figure S1G). USV call rates and call complexity follow distinct trajectories during the first two postnatal weeks. In contrast, altered USV dynamics have been identified in several mouse models of neurodevelopmental disorders (45,46). In line with these reports, the call rate of Df16 mice was reduced and peaked earlier (P7) when compared to Wt mice (peak at around P8; Figure 1B). Moreover, calls of Df16 mice showed reduced duration and complexity as well as altered proportions of call types (*i.e.* single frequency, frequency jump, and multiple steps calls) with a tendency towards simpler calls when compared to those of Wt mice (Figure 1C,D, Figure S1G). These results show that Df16 mice have early behavioral deficits when compared to Wt.

2.2. Altered microglial density and morphology in *Df(16)A*$^{+/-}$ mice during early development

Next, we monitored microglial characteristics along development by assessing the density and morphology of microglia in the PFC of Df16 and Wt mice (Figure 1E-H). We focused our analysis on the superficial layers (*i.e.* mainly layer 2/3) of the PFC (PFC_{SUP}) on the basis of their reported vulnerability to dysfunction in neuropsychiatric disorders (47). We found that microglia density increased from P4 to P12 in both groups, but this increase was more prominent in Df16 mice (*e.g.* at P8 ($p=0.0073$) and at P12 ($p=0.00034$)) when compared to Wt mice (Figure 1F). Additionally, at P12, microglia showed profound morphological alterations in Df16 mice, such as increased cell perimeter ($p=3.69\times10^{-6}$; Figure 1G), reduced cell eccentricity ($p=0.0046$; Figure 1G), increased cell spread ($p=1.82\times10^{-7}$; Figure S2D), and increased cell area ($p=2.7\times10^{-8}$; Figure S2E). These results indicate altered inflammatory states and, potentially, differences in microglial signaling in the PFC of neonatal Df16 mice.

2.3. Altered inflammatory signaling in *Df(16)A*$^{+/-}$ mice and its rescue by minocycline treatment during early development

Abnormal features of microglia might indicate altered neuroinflammatory states in the PFC of Df16 mice. To test this hypothesis, we quantified the expression of pro-inflammatory (*i.e.* tumor necrosis factor α (TNFα), complement 3 (C3), and complement 1q (C1q)) and neuroprotective (*i.e.* cluster of differentiation 47 (CD47)) markers as punctae in the PFC_{SUP} of Wt and Df16 mice (Figure 2A,B). In Wt PFC_{SUP}, these markers show an overall punctate expression (Figure 2A), largely colocalizing with synapses (Figure S2R), while only a small number of punctae are found within microglia or astrocytes (Figure S2Q,S). In the PFC_{SUP} of Df16, punctate expression of markers was maintained (Figure 2B), yet we observed an overall shift towards increased expression of pro-inflammatory markers at both RNA and protein levels (Figure 2D, Figure S2F-J). Specifically, punctae density for the pro-inflammatory markers TNFα ($p=7.08x10^{-7}$), C3 ($p=4.8x10^{-4}$), and C1q ($p=8.94x10^{-4}$) were increased, while expression of the neuroprotective marker CD47 was reduced (p=0.0104; Figure 2D). Additionally, we observed a distinct expression pattern for C1q, a component of the classical complement pathway that is involved in the tagging of synapses for microglial pruning (48,49). Overall C1q punctae density increase in PFC_{SUP} was accompanied by strong clustering of C1q in microglia of P12 Df16 mice that was not detected in age-matched Wt mice ($p=1.56x10^{-7}$; Figure 2E). This increased C1q accumulation in prefrontal microglia was detected in all investigated Df16 mice throughout early development and was largely concentrated in microglial lysosomes (Figure S2T).

Altered microglial reactivity might lead to excessive synaptic pruning. Accordingly, we tested the hypothesis that the observed shift in neuroinflammatory signaling during early development might affect spine densities of prefrontal pyramidal neurons, as has been previously reported for other models of neuropsychiatric disorders (20,50–52). We injected a viral vector (rAAV9_mCaMK2-eGFP-WPRE) into the PFC of P1 Wt and Df16 mice and quantified spine densities of eGFP-labeled L2/3 pyramidal neurons at P12 (Figure 2F). We detected a significant reduction of spine densities on dendrites of L2/3 pyramidal neurons of Df16 mice (p=0.011) compared to Wt mice (Figure 2F). This spine sparsification was more prominent for distal (distal basal: p=0.0197; distal apical: p=0.0028; Figure S2K,M,N) than for proximal branches (Figure S2L,O,P).

Next, we asked whether restoring the balance between pro-inflammatory and neuroprotective signaling might have an ameliorating effect on morphological and neuroanatomical deficits. Minocycline, an antibiotic with anti-inflammatory effects (53), has received increased attention in recent years due to its reported beneficial effects in the treatment of neuropsychiatric disorders in patients (54–63) and disease-relevant dysfunctions in mouse models (20,64,65). *In vitro*, minocycline directly affects uptake of synapses by microglia (15). Here, we administered minocycline from P4 to P12 via the drinking water of the dam. Immediately after the treatment (*i.e.* P12), we compared the expression of pro-inflammatory and neuroprotective markers in minocycline-treated Df16 mice (referred to as Df_{mino} hereafter) to Wt and untreated Df16 mice (Figure 2C-E, Figure S2). Minocycline largely rescued the expression of assessed markers when compared to Df16 (punctae densities: TNFα ($p=1.82x10^{-7}$), C3 (p=0.0023), C1q (p=0.015), CD47 (p=0.0082; Figure 2D, Figure S2G-J). Minocycline partially rescued C1q over-accumulation in microglia of Df_{mino} mice when compared to Df16 (p=0.013) and Wt ($p=2.26x10^{-5}$; Figure 2E). Moreover, minocycline treatment reduced the density of microglia cells in PFC_{SUP} of P12 Df_{mino} mice to a level comparable to that in Wt mice (Figure S2A). Microglial morphological features (*i.e.* eccentricity, perimeter, area, and spread) were comparable in Wt and Df_{mino} (Figure S2B-E). Lastly, spine densities on L2/3 pyramidal neurons of Df_{mino} mice were similar to those quantified for Wt while differing from Df16 mice (spine density overall: $p=2.14x10^{-4}$; distal basal: p=0.0021; distal apical: $p=8.06x10^{-7}$; Figure 2F, Figure S2K-P).

Altogether, these results indicate a shift towards pro-inflammatory signaling in Df16 mice during early development, resulting in a reduction of spines on dendrites of prefrontal L2/3 pyramidal neurons. Minocycline treatment during the first two postnatal weeks rebalances pro-inflammatory and neuroprotective signaling, leading to rescue of neuronal spine densities.

2.4. Abnormal neuronal activity in neonatal *Df(16)A*$^{+/-}$ mice and its rescue by minocycline

Reduction of spine densities on dendrites of L2/3 pyramidal neurons as a result of an imbalance in neuroinflammatory signaling might have major effects on circuit function, and especially on neuronal firing patterns in neonatal Df16 mice. To quantify potential deficits, we performed *in vivo* extracellular recordings from the PFC of head-fixed non-anesthetized P12 mice using Neuropixels probes (Figure 3). The detected reduction in number of units ($p=6.12x10^{-4}$) and spike density (total spikes per PFC recording channel; $p=0.0074$) in Df16 mice compared to Wt mice indicated a highly significant decrease of prefrontal firing (Figure 3C). Although at this age the firing features of putative pyramidal neuron vs. putative interneurons are indistinguishable, it is likely that the detected decrease in firing is mainly due to the dysfunction of excitatory pyramidal neurons, which make up ~80% of neocortical neurons (66). The overall firing rates of individual units were not different between Wt and Df16 mice (Figure S3A).

Next, to assess the strength of pairwise interactions between prefrontal neurons, we calculated the spike-time tiling coefficient (STTC), a measure that is unbiased by firing rate (67). Overall, STTC values did not differ between Wt and Df16 mice (Figure S3B). In all investigated mice, STTC values were higher for nearby neurons and decreased as a function of distance (Figure 3D). However, this decay was more pronounced in Df16 mice when compared to Wt mice (Figure 3D). This effect might be the result of the pronounced spine reduction on more distal apical dendrites, which are particularly important for integrating cortico-cortical connections (68). Lastly, we recorded local field potentials (LFP) in the PFC of non-anesthetized P12 Wt, Df16, and Df_{mino} mice using multi-site silicon probes (Figure S3C,D). The broadband power of prefrontal activity was significantly reduced in Df16 mice when compared to Wt mice ($p=0.015$; Figure S3D).

Early minocycline treatment largely rescued abnormal firing and local coupling patterns detected in P12 Df16 mice. Number and density of spiking neurons were comparable in Wt and Df_{mino} mice. STTC in Df_{mino} mice decreased with distance, but the deficit detected in Df16 mice was overcompensated by minocycline administration. Moreover, early minocycline treatment restored the broadband power of prefrontal activity, the recorded LFP being similar in P12 Wt and Df_{mino} mice (Figure S3D).

Thus, in addition to morphological deficits as a result of altered inflammatory signaling, Df16 mice show abnormal patterns of prefrontal activity and coupling during neonatal development, which are rescued by early administration of minocycline.

2.5. Long-lasting rebalancing of neuroinflammatory markers and rescue of neuroanatomical features by early minocycline treatment

Next, we asked whether the pro-inflammatory shift and neuronal dysfunction in Df16 mice persists throughout development. For this, we examined neuroinflammatory signaling markers and microglia morphological features in Wt and Df16 mice towards the end of development (*i.e.* P36) (Figure 4). No significant differences in microglia density and morphological parameters (*i. e.* cell spread, eccentricity, cell perimeter, and cell area) were detected between groups (Figure 4B, Figure S4A). In contrast, some differences in the molecular markers of

neuroinflammatory signaling cascades still persisted. The previously reported augmented punctae density of the pro-inflammatory marker C1q persisted in PFC_{SUP} of P36 Df16 mice (p=0.0012; Figure 4F). Similarly, an increased accumulation of C1q in PFC_{SUP} microglia was observed in P36 Df16 mice when compared to Wt mice (p=0.041; Figure 4G). In contrast, CD47, C3, and TNFα showed similar expression levels in Wt and Df16 mice (Figure 4C-E, Figure S4B-D). In line with this reduced but lasting imbalance of signaling cascades, spine densities on prefrontal L2/3 pyramidal neurons remained decreased in P36 Df16 mice when compared to Wt mice (p=0.0078). As shown for P12 Df16 mice, this spine reduction was particularly prominent on distal apical branches (p=0.0019; Figure S5C).

As some of the observed abnormalities lasted from neonatal to later development, we asked whether the observed ameliorating effects of early, transient minocycline treatment also persisted. Minocycline given to mice from P4 to 12 led to a partial rescue of C1q expression (p=0.025) and C1q accumulation in prefrontal microglia, as well as an increase of C3 expression (p=0.0062), while having no effect on TNFα expression (Figure 4D-G, Figure S4C-E). Early minocycline treatment not only rescued the neuroanatomical deficits but even slightly increased overall spine densities in Df_{mino} when compared to Df16 mice ($p=2.85x10^{-4}$; Figure 4H, Figure S5A-D).

Overall, we observed a less striking but persisting imbalance of inflammatory signaling as well as morphological deficits in Df16 mice towards the end of adolescent development, which were largely rescued by early minocycline treatment.

2.6. Long-lasting dysfunction of prefrontal circuits and related cognitive abilities in *Df(16)A*$^{+/-}$ mice and their rescue by early minocycline treatment

The observed persistence of neuroanatomical deficits throughout development might also have long-lasting effects on the function of prefrontal circuits. Indeed, abnormal neuronal activity and communication patterns have been identified in 22q11.2ds mouse models at adult age (43,44). To assess whether cellular and circuit deficits are also present at young adulthood, we recorded the LFP and spiking activity in the PFC of head-fixed non-anesthetized P42-44 Wt and Df16 mice (Figure 5A-D, Figure S5E). While no significant differences in firing rates of prefrontal neurons were detected when comparing Wt and Df16 mice (Figure S5E), the network activity was compromised. Df16 mice showed significantly (p=0.0391) reduced power in the beta (12-30 Hz) frequency band, while theta and gamma activity did not differ compared to Wt mice (Figure 5D). Early minocycline treatment rescued beta band activity to a level comparable to that of Wt mice (Figure 5D). In line with the spine density increase detected in Df_{mino} mice (Figure 4H, Figure S5A-D), early minocycline treatment augmented the theta power when compared to Df16 (p=0.0043) but not compared to Wt mice (Figure 5D). Furthermore, we assessed the impact of minocycline treatment in wildtype mice (hereafter referred to as Wt_{mino}) in order to exclude potential off-target effects of minocycline treatment. No significant differences between untreated Wt and Wt_{mino} animals were found on the anatomical (Figure S5A-D), electrophysiological (Figure 5B-D, Figure S5E), and behavioral levels (Figure 5G, Figure S5F-L).

Cognitive impairment is a hallmark feature in 22q11.2ds patients as well as in Df16 mice at adult age and has been related to prefrontal circuit dysfunction (22,41). We assessed the ontogeny of cognitive deficits and monitored the behavior of Df16 during late development. First, we analyzed the behavior of P35 mice in an open field. While the locomotor activity was similar in all groups, Df_{mino} mice spent less time in the center of the open field when compared to Wt (p=0.0496) mice (Figure S5F,G). This might reflect a higher degree of anxiety in mice due to early minocycline treatment. However, no significant changes of time spent in the center

area were observed in Wt_{mino} compared to Wt animals (Figure S5H), excluding a broader, minocycline-induced off-target effect on anxiety. Second, we assessed the decision-making performance of P30 Wt and Df16 mice in a 4-choice attentional set-shifting task (Figure 5E). This task consists of an acquisition and a reversal phase (Figure 5F) and critically depends on prefrontal function [85]. In the acquisition phase of the task, no differences between Wt and Df16 mice were detected (Figure 5G). However, during the reversal phase, Df16 mice made significantly more preservative errors (p=0.002; Figure S5J), leading to an overall increase of incorrect trials (p=0.001, Figure 5G) and of required number of trials to reach criterion (p=0.0017; Figure S5I). Early minocycline treatment fully rescued cognitive performance of Df_{mino} mice in the task (Figure 5G, Figure S5H-L).

These results indicate that early minocycline treatment rescues the long-lasting functional and behavioral deficits that persist in Df16 mice.

3. Discussion

Microdeletions at the 22q11.2 locus represent a severe burden for affected individuals. A strikingly increased incidence of neuropsychiatric symptoms has been reported for individuals with 22q11.2ds (8). Moreover, numerous studies have emphasized the link between 22q11.2 microdeletions and susceptibility towards developing schizophrenia later in life (7,69). Convergently, neuropsychiatric disorders have been linked to altered inflammatory states of neuronal tissue (10–12,70,71), yet the underlying mechanisms are still poorly understood. A mechanistic understanding of the pathophysiological trajectories inherent to 22q11.2ds requires in-depth investigation of mouse models that mimic this syndrome. The *Df(16)A* mouse model, carrying a syntenic deletion to human 22q11.2 microdeletions, offers high construct and face validity (42) and, in adult animals, recapitulates many of the pathophysiological features described for 22q11.2ds patients on the functional, behavioral, and physiological level (22,42,43).

Here, we investigated *Df(16)A*$^{+/-}$ mice during postnatal development, aiming to identify early dysregulation of neuroinflammatory signaling and its morphological, functional, and behavioral consequences. We show that (i) already during early postnatal development *Df(16)A*$^{+/-}$ mice display an imbalance of neuroinflammatory signaling markers in the PFC accompanied by spine loss and firing deficits of pyramidal neurons in prefrontal layer 2/3 as well as abnormal innate behaviors, (ii) morphological deficits and functional impairments of prefrontal neuronal networks, reflected by disrupted patterns of activity, persisted until adulthood and were accompanied by reduced performance in a decision-making task, and (iii) transient minocycline treatment during early development largely rescued neuroinflammatory, behavioral, and electrophysiological deficits throughout development. These results emphasize the impact of neuroinflammatory signaling imbalance on cognitive function in a model of 22q11.2ds and provide potential targets and strategies for therapeutic intervention.

3.1. Imbalance of neuroinflammatory signaling cascades at the basis of early perturbations in *Df(16)A*$^{+/-}$ mice

Neuroinflammatory processes have been proposed as key contributors to the pathogenesis of neuropsychiatric disorders. Elevated levels of pro-inflammatory cytokines have been reported for patients and mouse models (72). This study reveals that already during early development, neuroinflammatory processes contribute to morphological, functional, and behavioral deficits of *Df(16)A*$^{+/-}$ mice that persist into adulthood. Altered microglial morphologies in PFC_{SUP} of *Df(16)A*$^{+/-}$ mice indicate changed reactive states (16), likely resulting from a distinct pro-inflammatory shift in prefrontal tissue. This corroborates previous reports of increased levels

of pro-inflammatory markers and oxidative stress in blood samples of 22q11.2ds patients (13,19). Previous studies proposed several cellular processes as potential underlying mechanisms for the neuropathological trajectories observed in 22q11.2ds mouse models. For example, thioredoxin reductase 2 (TXNRD2), one of the genes located within the affected chromosomal segment of 22q11.2 microdeletions, is involved in the catabolism of reactive oxygen species and TXNRD2 deletion leads to increased oxidative stress in neuronal tissue (73). Anti-oxidant treatment as well as restoring TXNRD2 expression in a 22q11.2ds mouse model was shown to rescue neuroanatomical deficits of prefrontal layer 2/3 neurons (73), providing a direct link between neuroinflammation and disruptions inherent to 22q11.2ds. Another notable pathway potentially underlying functional impairments in *Df(16)A*$^{+/-}$ mice is PI3K/Akt/Gsk3 signaling, which is essential in neurite polarization and growth during postnatal development (74). Inhibition of Gsk3 in *Df(16)A*$^{+/-}$ mice during development (P7-28) was shown to largely rescue working memory impairments as well as deficits of prefrontal-hippocampal synchrony (74). Disruption of this pathway in *Df(16)A*$^{+/-}$ mice has been attributed to distinct genes located within 22q11.2 microdeletions in different studies, *e.g.* disturbed protein trafficking due to deletion of palmitoyltransferase ZDHHC8 (74,75) or imbalanced dopaminergic signaling due to deletion of catechol-O-methyltransferase (COMT) (76,77). Notably, C1q, one of the pro-inflammatory markers highlighted in this study, can be directly linked to this pathway via its activation of PI3K (78) and therefore reveals an additional pathway by which Akt/Gsk3 signaling might be disturbed in *Df(16)A*$^{+/-}$ mice.

Among the components contributing to the shift in neuroinflammatory signaling in prefrontal tissue of *Df(16)A*$^{+/-}$ mice, C1q is of particular note. C1q is a component of the classical complement pathway and is essential for a wide array of functions, ranging from myelination during early development (79) to tagging of synapses for pruning in neurodegenerative disease (80). The complement signaling cascade has been previously implicated in the pathogenesis of 22q11.2ds, as increased levels of complement proteins, such as C3, have been reported in blood samples of 22q11.2ds patients (19), similar to the results shown here in prefrontal tissue of *Df(16)A*$^{+/-}$ mice. Moreover, we identified a distinct pattern of increased C1q accumulation in prefrontal microglia during early development of a 22q11.2ds model as a potential marker and, thus, as a potential target for future therapeutic interventions.

C1q has also been reported to specifically tag synapses for microglia-mediated pruning (49). As C1q accumulation in *Df(16)A*$^{+/-}$ prefrontal microglia was largely concentrated in lysosomes, it can be surmised that this accumulation is due to an increased number of C1q-tagged synapses being pruned specifically, thereby accounting at least partially for the reduced spine densities of L2/3 pyramidal neurons in *Df(16)A*$^{+/-}$ mice. Similarly, spine sparsification and decreased dendritic complexity has been reported for neurons of the deeper prefrontal layers (*i.e.* layer 5/6) in adult mice of 22q11.2ds models (22,26). Notably, C1q expression remains elevated throughout development while other signaling components (*i.e.* TNFα, C3, and CD47) normalize towards adolescence. This intrinsic normalization likely reflects a combination of compensatory mechanisms unfolding due to the chromosomal disruption inherent to the *Df(16)A*$^{+/-}$ model and developmental processes. As the healthy brain transitions from neonatal age (where components of immune, microglial, and inflammatory signaling cascades show peak expression levels (81–83)) into adolescent and adult stages, gene expression profiles as well as microglia themselves undergo maturation, including the intrinsic downregulation of pro-inflammatory mediators and concurrent upregulation of complement inhibition components (81,82,84). However, despite the observed normalization of several neuroinflammatory factors in *Df(16)A*$^{+/-}$ mice with age, persisting elevation of C1q suggests that subtle but functionally significant deviations might persist and contribute to long-term changes of connectivity, network function, and behavioral performance in *Df(16)A*$^{+/-}$ mice.

Furthermore, it can be postulated that the neuronal firing deficits at neonatal age underlie the long-lasting miswiring of prefrontal circuits as reflected by the abnormal spectral structure of network oscillations in young adult *Df(16)A*$^{+/-}$ mice, *i.e.*, decreased beta band power when compared to Wt mice. Oscillatory activity reflects coordinated neuronal dynamics primarily driven by synaptic activity, with slower frequencies emerging via long-range interactions between brain regions and faster frequencies resulting from within local circuits (85). In the developing PFC, the hippocampus provides excitatory inputs that drive the generation of theta band activity, whereas fast oscillatory activity in beta-gamma frequency range requires the activation of L2/3 pyramidal neurons (37,86,87). The observed decrease in beta frequency in the PFC of Df16 mice can be explained by reduced synaptic interactions within the recurrently connected L2/3 pyramidal neurons due to reduced spine densities. Notably, not only local but also long-range communication of the PFC seems to be disrupted in *Df(16)A*$^{+/-}$ mice, as adult *Df(16)A*$^{+/-}$ mice have been shown to display reduced hippocampal-prefrontal synchrony during working memory tasks (43). In light of these results, we propose that the cognitive impairments characteristic for 22q11.2 microdeletions arise from a complex sequence of morphological and functional deficits of prefrontal neurons that are initiated by a shift towards neuroinflammation in prefrontal tissue early in development.

3.2. Long-lasting rescue of morphological, functional, and behavioral deficits in Df(16)A$^{+/-}$ mice by minocycline

The present data demonstrate that early minocycline treatment causes broad and long-lasting rescue of deficits affecting *Df(16)A*$^{+/-}$ mice. Minocycline has a well-known anti-inflammatory effect and has been used mainly as an antibiotic in patient care (53). However, in recent years, minocycline has received increased attention due to its reported beneficial effects during treatment of patients with neuropsychiatric disorders (54). Especially the ameliorating effects of minocycline treatment on disrupted cognitive performance of *Df(16)A*$^{+/-}$ mice is a key aspect of this study, as 22q11.2ds patients show impaired PFC-dependent cognitive abilities (3,88). Minocycline has been used to ameliorate cognitive deficits in neuropsychiatric disorders and several clinical studies have shown beneficial effects of minocycline in schizophrenia patients (57,59,61–63). However, a lack of clear effect of minocycline treatment has also been reported (56,58). A possible explanation for these contradictory results might be divergent setups of the performed studies, including different choice of patient cohorts regarding their individual stages of psychosis, different sets of performed tests, as well as differing adjacent treatments. All of these factors might affect the effectiveness of minocycline treatment in neuropsychiatric disorders. Notably, a key aspect of minocycline treatment appears to be the chosen time point of treatment. In line with this, our results confirm the powerful effects of minocycline and showed that transient treatment early in life rescued most deficits detected in *Df(16)A*$^{+/-}$ mice throughout development.

These ameliorating effects might be explained by the known anti-inflammatory properties of minocycline, presenting an ideal candidate for restoring imbalanced neuroinflammatory signaling cascades, as we identified in *Df(16)A*$^{+/-}$ mice. This hypothesis is supported not only by the fact that minocycline has been found to restore normal microglial activity (65,89–92) but also by its direct effect on the complement cascade, specifically on C1q and C3 signaling (93). Additionally, the expression of TNFα, one of the components contributing to the pro-inflammatory shift in prefrontal tissue of P12 *Df(16)A*$^{+/-}$ mice, has been reported to be directly affected by minocycline application (60,94). Moreover, TNFα has been shown to increase nitric oxide synthase (NOS) activity (95,96), although the reported effects differ depending on assessed tissue or cell type (60,89,94–97), while minocycline was shown to inhibit NOS activity (97). Therefore, the increased expression levels of TNFα in the PFC of *Df(16)A*$^{+/-}$ mice

highlights a pathway through which pathophysiological trajectories during early development in *Df(16)A*$^{+/-}$ mice, and potentially in 22q11.2ds patients, could be modulated.

Fittingly, immediately after minocycline treatment, the observed imbalance of pro-inflammatory signaling in prefrontal tissue of *Df(16)A*$^{+/-}$ mice was restored and, consequently, microglia morphology, as well as neuroanatomy and neuronal activity were indistinguishable from that of wildtype mice. These beneficial effects of early minocycline treatment persisted throughout development (*i. e.* at P30, P36, and P44). Fittingly, minocycline-induced rescue of spine deficits restored beta band activity. The observed increase of theta band power after minocycline treatment might be due to an overcompensation of spine densities and perturbation of physiological pruning in the PFC. These results are in line with previous findings in a double-hit mouse model of schizophrenia combining a genetic risk factor (*i.e.* truncated DISC1) with an environmental stressor (*i.e.* maternal immune activation) (20). Of note: maternal immune activation as a known etiological factor of human neuropsychiatric disease (98) provides a direct link to inflammation, whereas the etiology of the *Df(16)A* model has a purely genetic basis. Therefore, we suggest that neuroinflammation early in life might represent a common mechanism underlying dysfunction and cognitive disability in multiple neuropsychiatric disorders. This might also explain the model-independent ameliorating effects of minocycline when applied during early development. Overall, in line with the complexity of 22q11.2ds etiology, the complex pathways underlying altered neuroinflammation might account for the striking impact of anti-inflammatory minocycline treatment that restores complement signaling via C1q and consequently, the prefrontal function in *Df(16)A*$^{+/-}$ mice.

In summary, our results highlight the crucial impact of neuroinflammatory signaling during early development on the pathophysiology of 22q11.2ds. As diagnosis of 22q11.2ds by genomic profiling is, as of yet, not standardized unless other parameters give medical indication for its presence, identifying the underlying molecular and cellular pathways of this disease remains an essential factor in developing future therapies. Along this line, anti-inflammatory treatment with minocycline early in life appears as a promising approach for restoring prefrontal function and cognitive integrity in a model of 22q11.2 deletion syndrome.

4. Availability of data and materials

All scripts and processed data on which the analysis is based are available on the following github repository: [to be added upon publication].

5. Competing interests

The authors declare that they have no competing interests.

6. Funding

This work was funded by grants from the German Research Foundation (Ha4466/20-1 to I.H.-O., Ha4466/22-1 to I.H.-O., and SFB936 178316478 to I.H.-O.).

7. Authors' contributions

I.H.-O. and A.G. conceived the study. A.G. designed the experiments. A.G., M.C., S.B, and A.M. carried out the experiments. A.G., M.C., and S.B. analyzed the data. A.G. and I.H.-O. wrote the manuscript. All authors discussed and commented on the manuscript.

8. Acknowledgements

We thank Dr. Joseph Gogos for providing the *Df(16)A* mouse line, and A. Dahlmann and P. Putthoff for their excellent technical assistance.

9. Methods

9.1. Animals

Animal experiments were carried out in accordance with German laws and regulations and the guidelines of the European community for the use of animals in research. Specific experiments were approved by the local ethical committee. Animals were group-housed under standard conditions with access to food and water *ad libitum* in a 12-hour light-dark cycle. A total of 129 mice of both sexes were investigated from P12 to P44. C57BL/6J mice were defined as control animals and heterozygous animals of the *Df(16)A*$^{+/-}$ line (B6.129S7-Del(16Dgcr2-Hira)3Aam) were investigated as a model of the 22q11.2 deletion syndrome (42). Due to nonviability of homozygous *Df(16)A*$^{+/-}$ animals and aiming to exclude potential effects due to the dam's genotype, breeding was carried out with wildtype dams and heterozygous *Df(16)A*$^{+/-}$ males. For all mice, the day of birth was considered as P0. Genotypes were assessed using genomic DNA isolated from tail biopsies from all pups (see supplementary). The *Df(16)A*$^{+/-}$ line does not correspond to mendelian distribution, since, as previously reported, ~ 11% of hemizygous pups die at birth (42). Cardiac abnormalities are likely to account for the early lethality. In a milder form, they persist in 18% of surviving pups, as shown for another mouse line mimicking the 22q11.2 microdeletion (99).

9.2. Minocycline treatment

In line with previous studies (20,64), dams received minocycline in their drinking water at a dose of 30mg/kg body weight per day, allowing for minocycline to be passed to pups via lactation. No difference in drinking behavior could be observed between dams receiving water with and dams receiving water without minocycline.

9.3. Immunohistochemistry

Mice were transcardially perfused with ice-cold phosphate-buffered saline (PBS), followed by paraformaldehyde (PFA; 4% (w/v) in PBS) before dissection. Tissue was prepared in 80µm sections using a vibratome. For IHC, sections were incubated in 0.3 H_2O_2 (v/v) for 30min at RT before blocking for 1h in PBS with 0.75% (v/v) TritonX-100, 5% (v/v) normal donkey serum, and 5% (v/v) normal goat serum. Subsequently, primary antibodies (see supplementary) were applied in PBS with 0.75% (v/v) TritonX-100, 1% (v/v) normal donkey serum, and 1% (v/v) normal goat serum at 4°C for 3d. After washing, secondary antibodies were applied in PBS with 0.75% (v/v) TritonX-100, 1% (v/v) normal donkey serum, and 1% (v/v) normal goat serum at RT for 4h. Fluorescence images were obtained with an inverted confocal microscope (Olympus FV1000), pre-processed using ImageJ software (ImageJ 1.46r, Wayne Rasband, US National Institutes of Health, Bethesda, Maryland), and analyzed using MATLAB (see supplementary methods).

9.4. Stereotaxic injection

For sparse infection of prefrontal neurons and subsequent tracing of spine densities, the viral vector rAAV9_mCaMK2α-eGFP-WPRE (addgene, 5x10^6 viral particles in 25 nl) was injected into the PFC (anteroposterior +1mm, mediolateral ±0.15mm, and dorsoventral -0.9mm from bregma) of both hemispheres of P1 mice. For this, a 33-gauge beveled NanoFil needle, a NanoFil syringe, and a MicroSyringe Pump Controller (World Precision Instruments, Sarasota,

Florida) were used. Viral suspension was infused at a rate of 10 nl/min. After surgery and recovery, pups were returned to their nest.

9.5. Ultrasonic vocalizations

Ultrasonic vocalizations were assessed under low light intensity and constant temperature according to established protocols (100,101). Pups were isolated from their dam and littermates and placed into an acoustically isolated chamber (20 x 15 x 10 cm) below a condenser microphone (CM16/CMPA, Avisoft Bioacoustics, Berlin, Germany). Vocalizations were recorded for 90 s at a sampling rate of 250 kHz using Avisoft UltraSoundGate 116 db (Avisoft Bioacoustics) with the corresponding software. Ultrasonic vocalizations were analyzed using DeepSqueak software in a MATLAB surrounding (102).

9.6. Attentional set-shifting task

Behavioral tests were performed during the light phase. A four-choice odor discrimination and reversal task was performed as previously described (40,103). Briefly, at P30, mice were habituated to a rectangular maze (30 x 30 cm) with four partially sectioned off compartments in each corner (walls: 7 cm). In each corner, a dish (Ø5 cm, 0.5 cm height) with unscented wood shavings and a piece of Cocoa Krispies was placed. Mice were allowed to explore the arena and the dishes freely for 20 min. During the pre-training phase, one dish with wood shavings and a treat was placed into one corner for the mouse to explore until the treat was found. Pre-training was repeated until the mouse was habituated to the paradigm in all four corners of the maze. For testing, the unscented wood shavings were replaced by wood shavings scented with dried spices (0.4 % (w/w) garlic, 0.4 % (w/w) black pepper, 0.4 % (w/w) rosemary, 0.4 % (w/w) thyme, or 0.2 % (w/w) clove; FUCHS Gewürze GmbH), one of which was rewarded with the familiar food reward. Mice had to discriminate among the four odors and learn which one to associate with the buried food reward. Trials were timed and considered concluded as soon as the mouse chose a dish which was scored based on digging (purposeful moving of wooden shaving with nose or paws). Between each trial, the positions of the dishes were switched among the four corners of the maze to remove locational bias. The acquisition phase was considered complete once mice performed 8 out of 10 consecutive trials correctly. Immediately upon completion of the acquisition phase, the reversal phase was started. One odor was switched for a new, unfamiliar odor (novel error), the previously rewarded odor was no longer rewarded (persevering error), one previously unrewarded odor remained unrewarded (irrelevant error), and one of the familiar, previously unrewarded odors now contained the familiar food reward (correct). The reversal phase was conducted in the exact same manner as the acquisition phase. The reversal phase was considered complete once the mouse performed 8 out of 10 consecutive trials correctly.

9.7. *In vivo* electrophysiology in P12 mice

Surgery. *In vivo* extracellular recordings were performed from the PFC of non-anesthetized P12 mice as previously described (104). The surgery was performed under isoflurane anesthesia (induction: 5%; maintenance: 1-2%) and preceded by the application of a local anesthetic on the neck muscles (0.5% bupivacain / 1% lidocaine). Neck muscles were cut to minimize muscle artifacts. A craniotomy over the PFC (0.5mm anterior to bregma, 0.1-0.5mm lateral to the midline) was performed by carefully thinning the skull and then removing it with the use of a motorized drill. Recordings were performed under head-fixed conditions, preventing head movement but permitting free movement of limbs. Mice were kept on a heated (37°) surface surrounded by cotton wool throughout the entire recording. One Neuropixels probe 1.0 phase 3B (Imec, Belgium) (angle 0°) was vertically inserted into the frontal lobe at a very low speed

(insertion time 20-30 minutes) and a depth of 4 mm. The tip of the probe was used as reference. Before signal acquisition, mice were allowed to recover for ~ 45-60 minutes, to maximize the quality and stability of the recording as well as single units' yield. Epifluorescence images of coronal brain sections containing the PFC were acquired post mortem to reconstruct the position of the DiI-stained recording electrode.

Signal acquisition. The signal was recorded using the Neuropixels head-stage 1.0 and Neuropixels 1.0 PXIe acquisition system (Imec, Belgium) through the OpenEphys interface and the Neuropixels plugin. The SUA signal was recorded at 30 kHz (*AP gain* = 500, *AP Filter Cut* = ON), whereas the LFP signal was recorded at a 2.5 kHz sampling rate (*LFP gain* = 250).

Spike sorting. Spike sorting was achieved using Kilosort 2.5 (*fshigh* = 500, *minFR* = 0.001, *spkTh* = -4, *sig* = 20, *nblocks* = 5). The automatically-obtained clusters were manually curated using phy (https://github.com/cortex-lab/phy). The manual spike sorting was done blindly to the mouse genotype / treatment.

SUA firing statistics

Firing rate. Firing rate (in Hz) was computed as the number of spikes divided by the total recording length in seconds.

Spike-Time Tiling Coefficient (STTC). The STTC (timescale of 10ms) was computed as follows (67):

$$STTC = \frac{1}{2}\left(\frac{P_A - T_B}{1 - P_A T_B} + \frac{P_B - T_A}{1 - P_B T_A}\right) \quad \text{(Eq. 1)}$$

where PA is the proportion of spikes of spike train A that occurs within ±Δt of a spike train B spike. TA is the proportion of time that occurs within (is "tiled" by) ±Δt from spikes of spike train A. The same applies for PB and TB. ±Δt is the lag parameter and was set at 10ms. The pairwise distance between units (*i.e.*, putative cell bodies) was computed as the vertical distance between the recording sites on which the two units were detected with maximum amplitude.

9.8. Electrophysiological recordings P42-44

Surgery. *In vivo* extracellular recordings were performed from the PFC of non-anesthetized P42-44 mice. A metal bar for head fixation was implanted under isoflurane anesthesia (induction: 5%, maintenance: 1-2%) one week before recording. The skull above the right PFC (coordinates from bregma: 0.8mm anterior, 0.8mm lateral) was exposed and the electrode insertion site was marked on the skull. A silver wire was implanted above the cerebellum as reference electrode. Mice received buprenorphine (0.1 mg/kg s.c.) and recovered in their home cage for 4-5 days after surgery before they were accustomed to handling and head fixation. A small craniotomy (<0.5 mm in diameter) above the PFC was performed under brief isoflurane anesthesia. Mice were head-fixed and kept in a plastic tube to allow free movement of limbs while preventing head movement. A 16-channel silicon probe (Neuronexus, USA) was inserted into the PFC (2.0 mm deep from the dura). To probe was stained with DiI (1,1'-Dioctadecyl-3,3,3',3'-tetramethylindocarbocyanine perchlorate, Molecular Probes, USA) to confirm the recoding position post mortem. Only recordings from confirmed location in the PFC were considered for analysis.

Signal acquisition. To ensure full recovery from anesthesia and settling of the silicon probe in the tissue, data acquisition started 40 min after electrode insertion. Extracellular signals were band-pass filtered (0.1-9000Hz) and digitized (32kHz) with a multichannel extracellular

amplifier (Digital Lynx SX, Neuralynx, USA) for 20-25 min. Some mice were used for 2 recording sessions on different days to reduce the animal numbers. In this case, the craniotomy was covered with silicon sealant between recordings. Distinct probe tracks in these mice make it unlikely that the same neurons were recorded across sessions. Data were analyzed with open source and custom-written algorithms in MATLAB R2021a and Python environments. For LFP analysis, data were band-pass filtered (1-100 Hz) using a phase preserving third-order Butterworth filter. Power spectral density was calculated using Welch's method with non-overlapping windows of 2s. Time-frequency power plots were calculated with a continuous wavelet transform (Morlet wavelet). Single unit activity was detected and sorted using Klusta (105) followed by manual curation in phy ().

9.9. Statistical modeling

Statistical modeling was carried out in the R environment. All scripts and processed data on which the analysis is based are available on the following github repository: [to be added upon publication]. Nested data (Figures 1, 2, 3, 4) were analyzed with linear mixed-effects models (*lmer* function of the *lme4* R package) with “mouse” as random effect, except for spine density analyses where “neuron” was used as random effect. Non-nested data were analyzed with linear models (*lm* function). The density of microglia inclusions (Figure 2), spike density (Figure 3), STTC (Figure 3), the LFP power at different frequency bands (Figure 5), which followed an approximately log-normal distribution, were log-transformed and analyzed with linear (mixed-effect) models. Statistical significance for linear mixed-effects models was computed with the *lmerTest* R package (106) and the *anova* R function. Statistical significance for linear models was computed with the *anova* R function. Model selection was performed according to experimental design. Post-hoc analysis was carried out using the *emmeans* and *emtrends* functions of the *emmeans* R package (107).

10. List of Supplementary Material

Supplementary materials and methods

Figure S1 to S5

Table S1 and S2

11. References

1. Mcdonald-Mcginn DM, Tonnesen MK, Laufer-Cahana A, Finucane B, Driscoll DA, Emanuel BS, et al. Phenotype of the 22q11.2 deletion in individuals identified through an affected relative: Cast a wide *FISH*ing net! Genet Med. 2001 Jan 1;3(1):23–9.

2. Cortés-Martín J, Peñuela NL, Sánchez-García JC, Montiel-Troya M, Díaz-Rodríguez L, Rodríguez-Blanque R. Deletion Syndrome 22q11.2: A Systematic Review. Children. 2022 Aug 3;9(8):1168.

3. Woodin M, Wang PP, Aleman D, McDonald-McGinn D, Zackai E, Moss E. Neuropsychological profile of children and adolescents with the 22q11.2 microdeletion. Genet Med. 2001 Jan 1;3(1):34–9.

4. Gothelf D, Presburger G, Levy D, Nahmani A, Burg M, Berant M, et al. Genetic, developmental, and physical factors associated with attention deficit hyperactivity disorder in patients with velocardiofacial syndrome. Am J Med Genet B Neuropsychiatr Genet. 2004;126B(1):116–21.

5. Gothelf D, Presburger G, Zohar AH, Burg M, Nahmani A, Frydman M, et al. Obsessive-compulsive disorder in patients with velocardiofacial (22q11 deletion) syndrome. Am J Med Genet B Neuropsychiatr Genet. 2004;126B(1):99–105.

6. Marshall CR, Noor A, Vincent JB, Lionel AC, Feuk L, Skaug J, et al. Structural Variation of Chromosomes in Autism Spectrum Disorder. Am J Hum Genet. 2008 Feb 8;82(2):477–88.

7. Pulver AE, Nestadt G, Goldberg R, Shprintzen RJ, Lamacz M, Wolyniec PS, et al. Psychotic Illness in Patients Diagnosed with Velo-Cardio-Facial Syndrome and Their Relatives. J Nerv Ment Dis. 1994 Aug;182(8):476.

8. Schneider M, Debbané M, Bassett AS, Chow EWC, Fung WLA, van den Bree MBM, et al. Psychiatric Disorders From Childhood to Adulthood in 22q11.2 Deletion Syndrome: Results From the International Consortium on Brain and Behavior in 22q11.2 Deletion Syndrome. Am J Psychiatry. 2014 Jun;171(6):627–39.

9. Mosheva M, Korotkin L, Gur RE, Weizman A, Gothelf D. Effectiveness and side effects of psychopharmacotherapy in individuals with 22q11.2 deletion syndrome with comorbid psychiatric disorders: a systematic review. Eur Child Adolesc Psychiatry. 2020 Aug 1;29(8):1035–48.

10. Baba H, Suzuki T, Arai H, Emson PC. Expression of nNOS and soluble guanylate cyclase in schizophrenic brain. NeuroReport. 2004 Mar 22;15(4):677.

11. Bitanihirwe BKY, Woo TUW. Oxidative Stress in Schizophrenia: An Integrated Approach. Neurosci Biobehav Rev. 2011 Jan 1;35(3):878–93.

12. Ishii T, Hattori K, Miyakawa T, Watanabe K, Hidese S, Sasayama D, et al. Increased cerebrospinal fluid complement C5 levels in major depressive disorder and schizophrenia. Biochem Biophys Res Commun. 2018 Mar 4;497(2):683–8.

13. Menghi M, Micangeli G, Tarani F, Putotto C, Pirro F, Mariani A, et al. Neuroinflammation and Oxidative Stress in Individuals Affected by DiGeorge Syndrome. Int J Mol Sci. 2023 Feb 20;24(4):4242.

14. Pinto B, Morelli G, Rastogi M, Savardi A, Fumagalli A, Petretto A, et al. Rescuing Over-activated Microglia Restores Cognitive Performance in Juvenile Animals of the Dp(16) Mouse Model of Down Syndrome. Neuron. 2020 Dec 12;108(5):887.

15. Sellgren CM, Gracias J, Watmuff B, Biag JD, Thanos JM, Whittredge PB, et al. Increased synapse elimination by microglia in schizophrenia patient-derived models of synaptic pruning. Nat Neurosci. 2019 Mar;22(3):374–85.

16. Arcuri C, Mecca C, Bianchi R, Giambanco I, Donato R. The Pathophysiological Role of Microglia in Dynamic Surveillance, Phagocytosis and Structural Remodeling of the Developing CNS. Front Mol Neurosci. 2017 Jun 19;10:191.

17. Gesuita L, Cavaccini A, Argunsah AÖ, Favuzzi E, Ibrahim LA, Stachniak TJ, et al. Microglia contribute to the postnatal development of cortical somatostatin-positive inhibitory cells and to whisker-evoked cortical activity. Cell Rep. 2022 Aug 16;40(7):111209.

18. Kaur C, Rathnasamy G, Ling EA. Biology of Microglia in the Developing Brain. J Neuropathol Exp Neurol. 2017 Sep 1;76(9):736–53.

19. Grinde D, Øverland T, Lima K, Schjalm C, Mollnes TE, Abrahamsen TG. Complement Activation in 22q11.2 Deletion Syndrome. J Clin Immunol. 2020;40(3):515–23.

20. Chini M, Pöpplau JA, Lindemann C, Carol-Perdiguer L, Hnida M, Oberländer V, et al. Resolving and Rescuing Developmental Miswiring in a Mouse Model of Cognitive Impairment. Neuron. 2020 Jan 8;105(1):60-74.e7.

21. Comer AL, Jinadasa T, Sriram B, Phadke RA, Kretsge LN, Nguyen TPH, et al. Increased expression of schizophrenia-associated gene C4 leads to hypoconnectivity of prefrontal cortex and reduced social interaction. PLOS Biol. 2020 Jan 14;18(1):e3000604.

22. Fénelon K, Xu B, Lai CS, Mukai J, Markx S, Stark KL, et al. The Pattern of Cortical Dysfunction in a Mouse Model of a Schizophrenia-Related Microdeletion. J Neurosci. 2013 Sep 11;33(37):14825–39.

23. Glantz LA, Lewis DA. Decreased dendritic spine density on prefrontal cortical pyramidal neurons in schizophrenia. Arch Gen Psychiatry. 2000 Jan;57(1):65–73.

24. Hill JJ, Hashimoto T, Lewis DA. Molecular mechanisms contributing to dendritic spine alterations in the prefrontal cortex of subjects with schizophrenia. Mol Psychiatry. 2006 Jun;11(6):557–66.

25. Kolluri N, Sun Z, Sampson AR, Lewis DA. Lamina-Specific Reductions in Dendritic Spine Density in the Prefrontal Cortex of Subjects With Schizophrenia. Am J Psychiatry. 2005 Jun;162(6):1200–2.

26. Tabata H, Mori D, Matsuki T, Yoshizaki K, Asai M, Nakayama A, et al. Histological Analysis of a Mouse Model of the 22q11.2 Microdeletion Syndrome. Biomolecules. 2023 Apr 27;13(5):763.

27. Xu B, Hsu PK, Stark KL, Karayiorgou M, Gogos JA. Derepression of a novel neuronal inhibitor is a major outcome of miRNA dysregulation due to 22q11.2 microdeletion. Cell. 2013 Jan 17;152(1–2):262–75.

28. Baron-Cohen S. The cognitive neuroscience of autism. J Neurol Neurosurg Psychiatry. 2004 Jul;75(7):945–8.

29. Stuchlik A, Sumiyoshi T. Cognitive Deficits in Schizophrenia and Other Neuropsychiatric Disorders: Convergence of Preclinical and Clinical Evidence. Front Behav Neurosci. 2014 Dec 23;8:444.

30. Leicht G, Vauth S, Polomac N, Andreou C, Rauh J, Mußmann M, et al. EEG-Informed fMRI Reveals a Disturbed Gamma-Band–Specific Network in Subjects at High Risk for Psychosis. Schizophr Bull. 2016 Jan;42(1):239–49.

31. Richter M, Murtaza N, Scharrenberg R, White SH, Johanns O, Walker S, et al. Altered TAOK2 activity causes autism-related neurodevelopmental and cognitive abnormalities through RhoA signaling. Mol Psychiatry. 2019;24(9):1329–50.

32. Kalemaki K, Velli A, Christodoulou O, Denaxa M, Karagogeos D, Sidiropoulou K. The developmental changes in intrinsic and synaptic properties of prefrontal neurons enhance local network activity from the second to the third postnatal weeks in mice. Cereb Cortex. 2022 Sep 1;32(17):3633–50.

33. Larsen B, Luna B. Adolescence as a neurobiological critical period for the development of higher-order cognition. Neurosci Biobehav Rev. 2018 Nov 1;94:179–95.

34. Pinto JG, Jones DG, Murphy KM. Comparing development of synaptic proteins in rat visual, somatosensory, and frontal cortex. Front Neural Circuits [Internet]. 2013 May 28 [cited 2024 Jul

15];7. Available from: https://www.frontiersin.org/journals/neural-circuits/articles/10.3389/fncir.2013.00097/full

35. Rinetti-Vargas G, Phamluong K, Ron D, Bender KJ. Periadolescent Maturation of GABAergic Hyperpolarization at the Axon Initial Segment. Cell Rep. 2017 Jul 5;20(1):21–9.

36. Bitzenhofer SH, Pöpplau JA, Chini M, Marquardt A, Hanganu-Opatz IL. A transient developmental increase in prefrontal activity alters network maturation and causes cognitive dysfunction in adult mice. Neuron. 2021 Apr 21;109(8):1350-1364.e6.

37. Bitzenhofer SH, Ahlbeck J, Wolff A, Wiegert JS, Gee CE, Oertner TG, et al. Layer-specific optogenetic activation of pyramidal neurons causes beta–gamma entrainment of neonatal networks. Nat Commun. 2017 Feb 20;8:14563.

38. Medendorp WE, Bjorefeldt A, Crespo EL, Prakash M, Pal A, Waddell ML, et al. Selective postnatal excitation of neocortical pyramidal neurons results in distinctive behavioral and circuit deficits in adulthood. iScience. 2021 Mar 19;24(3):102157.

39. Nabel EM, Garkun Y, Koike H, Sadahiro M, Liang A, Norman KJ, et al. Adolescent frontal top-down neurons receive heightened local drive to establish adult attentional behavior in mice. Nat Commun. 2020 Aug 7;11:3983.

40. Pöpplau JA, Schwarze T, Dorofeikova M, Pochinok I, Günther A, Marquardt A, et al. Reorganization of adolescent prefrontal cortex circuitry is required for mouse cognitive maturation. Neuron. 2024 Feb 7;112(3):421-440.e7.

41. McDonald-McGinn DM, Sullivan KE, Marino B, Philip N, Swillen A, Vorstman JAS, et al. 22q11.2 deletion syndrome. Nat Rev Dis Primer. 2015 Nov 19;1:15071.

42. Stark KL, Xu B, Bagchi A, Lai WS, Liu H, Hsu R, et al. Altered brain microRNA biogenesis contributes to phenotypic deficits in a 22q11-deletion mouse model. Nat Genet. 2008 Jun;40(6):751–60.

43. Sigurdsson T, Stark KL, Karayiorgou M, Gogos JA, Gordon JA. Impaired hippocampal–prefrontal synchrony in a genetic mouse model of schizophrenia. Nature. 2010 Apr 1;464(7289):763–7.

44. Mukherjee A, Carvalho F, Eliez S, Caroni P. Long-Lasting Rescue of Network and Cognitive Dysfunction in a Genetic Schizophrenia Model. Cell. 2019 Sep 5;178(6):1387-1402.e14.

45. Premoli M, Memo M, Bonini SA. Ultrasonic vocalizations in mice: relevance for ethologic and neurodevelopmental disorders studies. Neural Regen Res. 2020 Nov 27;16(6):1158–67.

46. Scattoni ML, Crawley J, Ricceri L. Ultrasonic vocalizations: A tool for behavioural phenotyping of mouse models of neurodevelopmental disorders. Neurosci Biobehav Rev. 2009 Apr 1;33(4):508–15.

47. Chini M, Hanganu-Opatz IL. Prefrontal Cortex Development in Health and Disease: Lessons from Rodents and Humans. Trends Neurosci. 2021 Mar 1;44(3):227–40.

48. Wang C, Yue H, Hu Z, Shen Y, Ma J, Li J, et al. Microglia mediate forgetting via complement-dependent synaptic elimination. Science. 2020 Feb 7;367(6478):688–94.

49. Györffy BA, Kun J, Török G, Bulyáki É, Borhegyi Z, Gulyássy P, et al. Local apoptotic-like mechanisms underlie complement-mediated synaptic pruning. Proc Natl Acad Sci U S A. 2018 Jun 12;115(24):6303–8.

50. Cooper MA, Koleske AJ. Ablation of ErbB4 from excitatory neurons leads to reduced dendritic spine density in mouse prefrontal cortex. J Comp Neurol. 2014 Dec 1;522(14):3351–62.

51. Gupta SC, Ravikrishnan A, Liu J, Mao Z, Pavuluri R, Hillman BG, et al. The NMDA receptor GluN2C subunit controls cortical excitatory-inhibitory balance, neuronal oscillations and cognitive function. Sci Rep. 2016 Dec 6;6:38321.

52. Lazaro MT, Taxidis J, Shuman T, Bachmutsky I, Ikrar T, Santos R, et al. Reduced Prefrontal Synaptic Connectivity and Disturbed Oscillatory Population Dynamics in the CNTNAP2 Model of Autism. Cell Rep. 2019 May 28;27(9):2567-2578.e6.

53. Dean OM, Data-Franco J, Giorlando F, Berk M. Minocycline. CNS Drugs. 2012 May 1;26(5):391–401.

54. Panizzutti B, Skvarc D, Lin S, Croce S, Meehan A, Bortolasci CC, et al. Minocycline as Treatment for Psychiatric and Neurological Conditions: A Systematic Review and Meta-Analysis. Int J Mol Sci. 2023 Mar 9;24(6):5250.

55. Ghoreishi A, Granpy S, Armani A. The Role of Minocycline in Neuro-Cognitive Symptoms in the Episodes of Primary Psychosis: A Clinical Trial. Acta Med Iran. 2020 Aug 10;194–8.

56. Weiser M, Levi L, Burshtein S, Chiriță R, Cirjaliu D, Gonen I, et al. The effect of minocycline on symptoms in schizophrenia: Results from a randomized controlled trial. Schizophr Res. 2019 Apr 1;206:325–32.

57. Chaudhry IB, Hallak J, Husain N, Minhas F, Stirling J, Richardson P, et al. Minocycline benefits negative symptoms in early schizophrenia: a randomised double-blind placebo-controlled clinical trial in patients on standard treatment. J Psychopharmacol (Oxf). 2012 Sep 1;26(9):1185–93.

58. Deakin B, Suckling J, Barnes TRE, Byrne K, Chaudhry IB, Dazzan P, et al. The benefit of minocycline on negative symptoms of schizophrenia in patients with recent-onset psychosis (BeneMin): a randomised, double-blind, placebo-controlled trial. Lancet Psychiatry. 2018 Nov 1;5(11):885–94.

59. Liu F, Guo X, Wu R, Ou J, Zheng Y, Zhang B, et al. Minocycline supplementation for treatment of negative symptoms in early-phase schizophrenia: A double blind, randomized, controlled trial. Schizophr Res. 2014 Mar 1;153(1):169–76.

60. Liu HY, Yue J, Hu LN, Cheng LF, Wang XS, Wang XJ, et al. Chronic minocycline treatment reduces the anxiety-like behaviors induced by repeated restraint stress through modulating neuroinflammation. Brain Res Bull. 2018 Oct 1;143:19–26.

61. Levkovitz Y, Mendlovich S, Riwkes S, Braw Y, Levkovitch-Verbin H, Gal G, et al. A Double-Blind, Randomized Study of Minocycline for the Treatment of Negative and Cognitive Symptoms in Early-Phase Schizophrenia. J Clin Psychiatry. 2009 Nov 3;70(2):4863.

62. Khodaie-Ardakani MR, Mirshafiee O, Farokhnia M, Tajdini M, Hosseini SMR, Modabbernia A, et al. Minocycline add-on to risperidone for treatment of negative symptoms in patients with stable schizophrenia: Randomized double-blind placebo-controlled study. Psychiatry Res. 2014 Mar 30;215(3):540–6.

63. Kelly DL, Sullivan KM, McEvoy JP, McMahon RP, Wehring HJ, Liu F, et al. Adjunctive Minocycline in Clozapine Treated Schizophrenia Patients with Persistent Symptoms. J Clin Psychopharmacol. 2015 Aug;35(4):374–81.

64. Dansie LE, Phommahaxay K, Okusanya AG, Uwadia J, Huang M, Rotschafer SE, et al. Long-lasting Effects of Minocycline on Behavior in Young but not Adult Fragile X Mice. Neuroscience. 2013 Aug 29;246:10.1016/j.neuroscience.2013.04.058.

65. Mattei D, Ivanov A, Ferrai C, Jordan P, Guneykaya D, Buonfiglioli A, et al. Maternal immune activation results in complex microglial transcriptome signature in the adult offspring that is reversed by minocycline treatment. Transl Psychiatry. 2017 May;7(5):e1120–e1120.

66. Markram H, Toledo-Rodriguez M, Wang Y, Gupta A, Silberberg G, Wu C. Interneurons of the neocortical inhibitory system. Nat Rev Neurosci. 2004 Oct;5(10):793–807.

67. Cutts CS, Eglen SJ. Detecting Pairwise Correlations in Spike Trains: An Objective Comparison of Methods and Application to the Study of Retinal Waves. J Neurosci. 2014 Oct 22;34(43):14288–303.

68. Fişek M, Herrmann D, Egea-Weiss A, Cloves M, Bauer L, Lee TY, et al. Cortico-cortical feedback engages active dendrites in visual cortex. Nature. 2023 May;617(7962):769–76.

69. Liu H, Abecasis GR, Heath SC, Knowles A, Demars S, Chen YJ, et al. Genetic variation in the 22q11 locus and susceptibility to schizophrenia. Proc Natl Acad Sci U S A. 2002 Dec 24;99(26):16859–64.

70. Fagan K, Crider A, Ahmed AO, Pillai A. Complement C3 Expression Is Decreased in Autism Spectrum Disorder Subjects and Contributes to Behavioral Deficits in Rodents. Complex Psychiatry. 2017;3(1):19–27.

71. Magdalon J, Mansur F, Teles e Silva AL, de Goes VA, Reiner O, Sertié AL. Complement System in Brain Architecture and Neurodevelopmental Disorders. Front Neurosci [Internet]. 2020 [cited 2022 Aug 10];14. Available from: https://www.frontiersin.org/articles/10.3389/fnins.2020.00023

72. Günther A, Hanganu-Opatz IL. Neuronal oscillations: early biomarkers of psychiatric disease? Front Behav Neurosci. 2022;16:1038981.

73. Fernandez A, Meechan DW, Karpinski BA, Paronett EM, Bryan CA, Rutz HL, et al. Mitochondrial Dysfunction Leads to Cortical Under-connectivity and Cognitive Impairment. Neuron. 2019 Jun 19;102(6):1127-1142.e3.

74. Tamura M, Mukai J, Gordon JA, Gogos JA. Developmental inhibition of Gsk3 rescues behavioral and neurophysiological deficits in a mouse model of schizophrenia predisposition. Neuron. 2016 Mar 2;89(5):1100–9.

75. Mukai J, Tamura M, Fénelon K, Rosen AM, Spellman TJ, Kang R, et al. Molecular substrates of altered axonal growth and brain connectivity in a mouse model of schizophrenia. Neuron. 2015 May 6;86(3):680–95.

76. Käenmäki M, Tammimäki A, Myöhänen T, Pakarinen K, Amberg C, Karayiorgou M, et al. Quantitative role of COMT in dopamine clearance in the prefrontal cortex of freely moving mice. J Neurochem. 2010 Sep;114(6):1745–55.

77. Choi SJ, Mukai J, Kvajo M, Xu B, Diamantopoulou A, Pitychoutis PM, et al. A Schizophrenia-Related Deletion Leads to KCNQ2-Dependent Abnormal Dopaminergic Modulation of Prefrontal Cortical Interneuron Activity. Cereb Cortex N Y NY. 2018 Jun;28(6):2175–91.

78. Benavente F, Piltti KM, Hooshmand MJ, Nava AA, Lakatos A, Feld BG, et al. Novel C1q receptor-mediated signaling controls neural stem cell behavior and neurorepair. Pera M, Bronner ME, Cortes D, Noble M, editors. eLife. 2020 Sep 7;9:e55732.

79. Yu Q, Zhang N, Guan T, Guo Y, Marzban H, Lindsey B, et al. C1q is essential for myelination in the central nervous system (CNS). iScience. 2023 Nov 23;26(12):108518.

80. Dejanovic B, Wu T, Tsai MC, Graykowski D, Gandham VD, Rose CM, et al. Complement C1q-dependent excitatory and inhibitory synapse elimination by astrocytes and microglia in Alzheimer's disease mouse models. Nat Aging. 2022 Sep;2(9):837–50.

81. Cengiz P, Zafer D, Chandrashekhar JH, Chanana V, Bogost J, Waldman A, et al. Developmental differences in microglia morphology and gene expression during normal brain development and in response to hypoxia-ischemia. Neurochem Int. 2019 Jul;127:137–47.

82. Sager REH, Walker AK, Middleton F, Robinson K, Webster MJ, Weickert CS. Trajectory of change in brain complement factors from neonatal to young adult humans. J Neurochem. 2021;157(3):479–93.

83. Catale C, Garel S. Microglia in early brain development: A window of opportunity. Curr Opin Neurobiol. 2025 Aug 1;93:103062.

84. Matcovitch-Natan O, Winter DR, Giladi A, Vargas Aguilar S, Spinrad A, Sarrazin S, et al. Microglia development follows a stepwise program to regulate brain homeostasis. Science. 2016 Aug 19;353(6301):aad8670.

85. Buzsáki G, Anastassiou CA, Koch C. The origin of extracellular fields and currents — EEG, ECoG, LFP and spikes. Nat Rev Neurosci. 2012 Jun;13(6):407–20.

86. Brockmann MD, Pöschel B, Cichon N, Hanganu-Opatz IL. Coupled oscillations mediate directed interactions between prefrontal cortex and hippocampus of the neonatal rat. Neuron. 2011 Jul 28;71(2):332–47.

87. Bitzenhofer SH, Pöpplau JA, Hanganu-Opatz I. Gamma activity accelerates during prefrontal development. Vinck M, Colgin LL, Perrenoud Q, Moore CI, editors. eLife. 2020 Nov 18;9:e56795.

88. Sobin C, Kiley-Brabeck K, Daniels S, Khuri J, Taylor L, Blundell M, et al. Neuropsychological Characteristics of Children with the 22q11 Deletion Syndrome: A Descriptive Analysis. Child Neuropsychol. 2005 Feb 1;11(1):39–53.

89. Long Y, Wang Y, Shen Y, Huang J, Li Y, Wu R, et al. Minocycline and antipsychotics inhibit inflammatory responses in BV-2 microglia activated by LPS via regulating the MAPKs/JAK-STAT signaling pathway. BMC Psychiatry. 2023;23(1).

90. Cheng D, Qin ZS, Zheng Y, Xie JY, Liang SS, Zhang JL, et al. Minocycline, a classic antibiotic, exerts psychotropic effects by normalizing microglial neuroinflammation-evoked tryptophan-kynurenine pathway dysregulation in chronically stressed male mice. Brain Behav Immun. 2023 Jan 1;107:305–18.

91. Li X, Hu B, Guan X, Wang Z, Zhou Y, Sun H, et al. Minocycline protects against microgliopathy in a Csf1r haplo-insufficient mouse model of adult-onset leukoencephalopathy with axonal spheroids and pigmented glia (ALSP). J Neuroinflammation. 2023 May 31;20(1):134.

92. Yousefpour N, Locke S, Deamond H, Wang C, Marques L, St-Louis M, et al. Time-dependent and selective microglia-mediated removal of spinal synapses in neuropathic pain. Cell Rep. 2023 Jan 31;42(1):112010.

93. Zheng Y, Fan L, Xia S, Yang Q, Zhang Z, Chen H, et al. Role of complement C1q/C3-CR3 signaling in brain injury after experimental intracerebral hemorrhage and the effect of minocycline treatment. Front Immunol. 2022 Sep 15;13:919444.

94. Lee SM, Yune TY, Kim SJ, Kim YC, Oh YJ, Markelonis GJ, et al. Minocycline inhibits apoptotic cell death via attenuation of TNF-α expression following iNOS/NO induction by lipopolysaccharide in neuron/glia co-cultures. J Neurochem. 2004;91(3):568–78.

95. Madrigal JLM, Hurtado O, Moro MA, Lizasoain I, Lorenzo P, Castrillo A, et al. The Increase in TNF-α Levels Is Implicated in NF-κB Activation and Inducible Nitric Oxide Synthase Expression in Brain Cortex after Immobilization Stress. Neuropsychopharmacology. 2002 Feb;26(2):155–63.

96. Medeiros R, Prediger RDS, Passos GF, Pandolfo P, Duarte FS, Franco JL, et al. Connecting TNF-α Signaling Pathways to iNOS Expression in a Mouse Model of Alzheimer's Disease: Relevance for the Behavioral and Synaptic Deficits Induced by Amyloid β Protein. J Neurosci. 2007 May 16;27(20):5394–404.

97. Liu F, Zhang B, Xie L, Ruan Y, Xu X, Zeng Y, et al. Changes in plasma levels of nitric oxide metabolites and negative symptoms after 16-week minocycline treatment in patients with schizophrenia. Schizophr Res. 2018 Sep 1;199:390–4.

98. Han VX, Patel S, Jones HF, Dale RC. Maternal immune activation and neuroinflammation in human neurodevelopmental disorders. Nat Rev Neurol. 2021 Sep;17(9):564–79.

99. Lindsay EA, Botta A, Jurecic V, Carattini-Rivera S, Cheah YC, Rosenblatt HM, et al. Congenital heart disease in mice deficient for the DiGeorge syndrome region. Nature. 1999 Sep;401(6751):379–83.

100. Schepanski S, Chini M, Sternemann V, Urbschat C, Thiele K, Sun T, et al. Pregnancy-induced maternal microchimerism shapes neurodevelopment and behavior in mice. Nat Commun. 2022 Aug 5;13:4571.

101. Parbst F, Kostka JK, Günther A, Chen YN, Hanganu-Opatz IL, Bitzenhofer SH. Developmental Olfactory Dysfunction and Abnormal Odor Memory in Immune-Challenged Disc1+/− Mice. J Neurosci [Internet]. 2025 Jun 18 [cited 2025 Aug 12];45(25). Available from: https://www.jneurosci.org/content/45/25/e1007242025

102. Coffey KR, Marx RE, Neumaier JF. DeepSqueak: a deep learning-based system for detection and analysis of ultrasonic vocalizations. Neuropsychopharmacology. 2019 Apr;44(5):859–68.

103. Johnson C, Wilbrecht L. Juvenile mice show greater flexibility in multiple choice reversal learning than adults. Dev Cogn Neurosci. 2011 Jun 1;1(4):540–51.

104. Chini M, Hnida M, Kostka JK, Chen YN, Hanganu-Opatz IL. Preconfigured architecture of the developing mouse brain. Cell Rep. 2024 Jun 25;43(6):114267.

105. Rossant C, Kadir SN, Goodman DFM, Schulman J, Hunter MLD, Saleem AB, et al. Spike sorting for large, dense electrode arrays. Nat Neurosci. 2016 Apr;19(4):634–41.

106. Kuznetsova A, Brockhoff PB, Christensen RHB. lmerTest Package: Tests in Linear Mixed Effects Models. J Stat Softw. 2017 Dec 6;82(1):1–26.

924 107. Lenth RV, Buerkner P, Herve M, Love J, Riebl H, Singmann H. emmeans: Estimated Marginal
925 Means, aka Least-Squares Means [Internet]. 2020 [cited 2021 Feb 2]. Available from:
926 https://CRAN.R-project.org/package=emmeans

927

928

929 **Figure 1. Behavioral and microglial deficits in *Df(16)A*$^{+/-}$ mice during the first two postnatal weeks.** (**A**)
930 Schematic of the USV recording setup (top) and USV call classification (bottom). (**B**) Age-dependence of call
931 rates in Wt (gray, n=12) and Df16 (orange, n=11) mice. Solid lines depict median values and shaded areas
932 correspond to the standard error of the mean (s.e.m.). Significance is indicated by a black bar. (**C**) Call duration of
933 different call types (single frequency, frequency jump, and multiple steps calls) in Wt (gray) and Df16 (orange)
934 mice. (**D**) Proportion (in %) of single frequency, frequency jump, and multiple steps calls detected for P5-12 Wt
935 (n=12) and Df16 (n=11) mice. (**E**) Co-labeling of microglia (Iba1, green) and neuronal cell bodies (NeuN, red) in
936 coronal sections of PFC_{SUP} from P12 Wt (top) and Df16 (bottom) mice. Bars = 100 µm. (**F**) Microglia density in
937 PFC_{SUP} of P4, P8, and P12 Wt (gray) and Df16 (orange) mice. (**G**) Morphological features of microglia in P12 Wt
938 (gray) and Df16 (orange) mice. Left, perimeter of microglial cells. Right, eccentricity of microglial cells. Data in
939 violin plots are displayed as median (light gray) and box plots (dark gray) with 25th and 75th percentile. Colored
940 dots indicate individual data points, colored areas represent probability density of the variable. Significant
941 differences are indicated as *, **, *** for p<0.05, 0.01, 0.001, respectively. For detailed statistics see
942 Supplementary Table S1.

943

944 **Figure 2. Altered inflammatory signaling and its rescue by early minocycline treatment in neonatal**
945 ***Df(16)A*$^{+/-}$ mice.** (**A-C**) Representative confocal images showing co-labeling of Iba1 (green) and molecular
946 markers of neuroprotective (CD47) and pro-inflammatory (TNFα, C3, and C1q) markers (red) in the PFC_{SUP} of
947 P12 (A) Wt, (B) Df16, and (C) Df_{mino} mice. For each panel, solid boxes mark areas of higher magnification shown
948 on the right. (**D**) Quantification of CD47, TNFα, C3, and C1q-positive punctae in PFC_{SUP} of P12 Wt (gray), Df16
949 (orange), and Df_{mino} (green) mice. (n=6 mice, 2 areas per animal). (**E**) C1q inclusions in microglia of P12 Wt,
950 Df16, and Df_{mino} mice. Left, representative reconstructions of microglia and C1q based on Iba1 (gray) and C1q
951 (red) co-staining in Wt, Df16, and Df_{mino} mice. Right, quantification of C1q inclusion volume in microglia of P12
952 Wt (gray), Df16 (orange), and Df_{mino} (green) mice. (n=6 mice, 3 cells per animal). (**F**) Quantification of spines on
953 dendrites of prefrontal L2/3 pyramidal neurons after bilateral injection of rAAV9_mCaMK2α-eGFP-WPRE into
954 the PFC of P1 Wt, Df16, and Df_{mino} mice. Left, example images showing dendritic segments and spines from P12
955 Wt, Df16, and Df_{mino} mice at P12. Right, overall spine densities (including segments from apical and basal
956 dendrites as well as from proximal and distal branches for each neuron) of L2/3 pyramidal neurons in P12 Wt
957 (gray), Df16 (orange), and Df_{mino} (green) mice. (n=4 mice, 3 cells per animal). Data in violin plots are displayed
958 as median (light gray) and box plots (dark gray) with 25th and 75th percentile. Colored dots indicate individual data
959 points, colored areas represent probability density of the variable. Bars = 5 µm. Significant differences are
960 indicated as *, **, *** for p<0.05, 0.01, 0.001, respectively. For detailed statistics see Supplementary Table S1.

961

962 **Figure 3. Abnormal prefrontal firing patterns in neonatal *Df(16)A*$^{+/-}$ mice and its rescue by minocycline**
963 **treatment.** (**A**) Raster plots of spiking activity recorded in the PFC of P12 Wt (gray), Df16 (orange), and Df_{mino}
964 (green) mice. (**B**) Reconstruction of the DiI-labeled Neuropixels probe (red) superimposed on a NeuN-stained
965 (blue) coronal section including the PFC. Dotted lines mark the borders of prefrontal subdivisions cingulate (Cg),
966 prelimbic (PL), and infralimbic (IL) cortices. Solely recording sites in PL and IL were considered for the analysis.
967 (**C**) Violin plots displaying the density of units (left) and the log_{10}-transformed density of spikes (right) for P12
968 Wt (n=10), Df16 (n=11) and Df_{mino} (n=7) mice. Colored dots represent individual mice. (**D**) Line plot displaying
969 log-transformed STTC as a function of the distance between units, *i.e.*, putative cell bodies. Data are presented as
970 mean and 95% confidence interval. Data in violin plots (C, D) are displayed as median (light gray) and box plots
971 (dark gray) with 25th and 75th percentile. Colored dots indicate individual data points, colored areas represent
972 probability density of the variable. Significant differences are indicated as *, **, *** for p<0.05, 0.01, 0.001,
973 respectively. For detailed statistics see Supplementary Table S1.

974

Figure 4. Long-lasting impairment of neuroinflammatory signaling and neuronal morphology in *Df(16)A*$^{+/-}$ mice and rescue by early minocycline treatment.

(**A**) Representative confocal images of Iba1-labeled microglia (green) in the PFC_{SUP} of P36 Wt, Df16, and Df_{mino} mice. (**B**) Violin plot displaying the microglia density in the PFC_{SUP} of P36 Wt (gray), Df16 (orange), and Df_{mino} (green) mice. (**C-F**) Violin plots displaying the densities of (C) CD47-, (D) TNFα-, (E) C3-, and (F) C1q-positive punctae in the PFC_{SUP} of P36 Wt (gray), Df16 (orange), and Df_{mino} (green) mice. (n=6, 2 areas per animal). (**G**) C1q inclusions in microglia of P36 Wt, Df16, and Df_{mino} mice. Left, representative reconstructions of microglia and C1q inclusions based on Iba1 (gray) and C1q (red) co-staining in the PFC of Wt, Df16, and Df_{mino} mice. Right, violin plot of C1q inclusion volume in prefrontal microglia of P36 Wt (gray), Df16 (orange), and Df_{mino} (green) mice. (n=6, 3 cells per animal). (**H**) Quantification of spines on dendrites of prefrontal L2/3 pyramidal neurons after bilateral injection of rAAV9_mCaMK2α-eGFP-WPRE into the PFC of P1 Wt, Df16, and Df_{mino} mice. Overall spine densities are shown (including segments from apical and basal dendrites as well as from proximal and distal branches for each neuron) for P36 Wt (gray), Df16 (orange), and Df_{mino} (green) mice (n=4 mice, 3 cells per animal). Data in violin plots are displayed as median (light gray) and box plots (dark gray) with 25th and 75th percentile. Colored dots indicate individual data points, colored areas represent probability density of the variable. Bars = 5 µm. Significant differences are indicated as *, **, *** for $p<0.05$, 0.01, 0.001, respectively. For detailed statistics see Supplementary Table S1.

Figure 5. Long-lasting network and cognitive deficits in *Df(16)A*$^{+/-}$ mice and their rescue by early minocycline application. (**A**) Reconstruction of the DiI-labeled Neuropixels probe (red) superimposed on a NeuN-stained (blue) coronal section. Prefrontal subdivisions are indicated for cingulate (Cg), prelimbic (PL), and infralimbic (IL) cortices. (**B**) Representative extracellular recordings of electrophysiological activity from the PFC filtered at 1-100 Hz and corresponding wavelet spectra for a Wt (gray), Df16 (orange), Wt_{mino} (blue), and Df_{mino} (green) mouse at P42-44. (**C**) Power spectra of PFC activity in P42-44 Wt (gray, n=9 recordings from 7 mice), Df16 (orange, n=10 recordings from 7 mice), Wt_{mino} (blue, n=10 recordings from 6 animals), and Df_{mino} (green, n=9 recordings from 5 mice) mice. S.e.m. is indicated by shaded areas. (**D**) Power of PFC activity in theta (4-12 Hz), beta (12-30 Hz), and gamma (30-100 Hz) frequency in Wt (gray), Df16 (orange), Wt_{mino} (blue), and Df_{mino} (green) mice at P42-44. (**E**) Timeline for minocycline application and subsequent test in behavioral paradigms and electrophysiological recordings. (**F**) Phases of the attentional set-shifting task. (**G**) Trial duration and number of error trials during acquisition and reversal phase of the attentional set-shifting task for Wt (gray, n=12), Df16 (orange, n=12), Wt_{mino} (blue, n=9), and Df_{mino} (green, n=12) mice at P30. Data in violin plots are displayed as median (light gray) and box plots (dark gray) with 25th and 75th percentile. Colored dots indicate individual data points, colored areas represent probability density of the variable. Significant differences are indicated as *, **, *** for $p<0.05$, 0.01, 0.001, respectively. For detailed statistics see Supplementary Table S1.

Highlights

- Early postnatal pro-inflammatory shift in PFC of *Df(16)*$^{+/-}$ mice causes lasting deficits
- C1q accumulation marks microglia of *Df(16)*$^{+/-}$ mice throughout development
- Early, transient minocycline application restores microglial and neuroinflammatory signaling
- Minocycline lastingly rescues cognitive and electrophysiological deficits

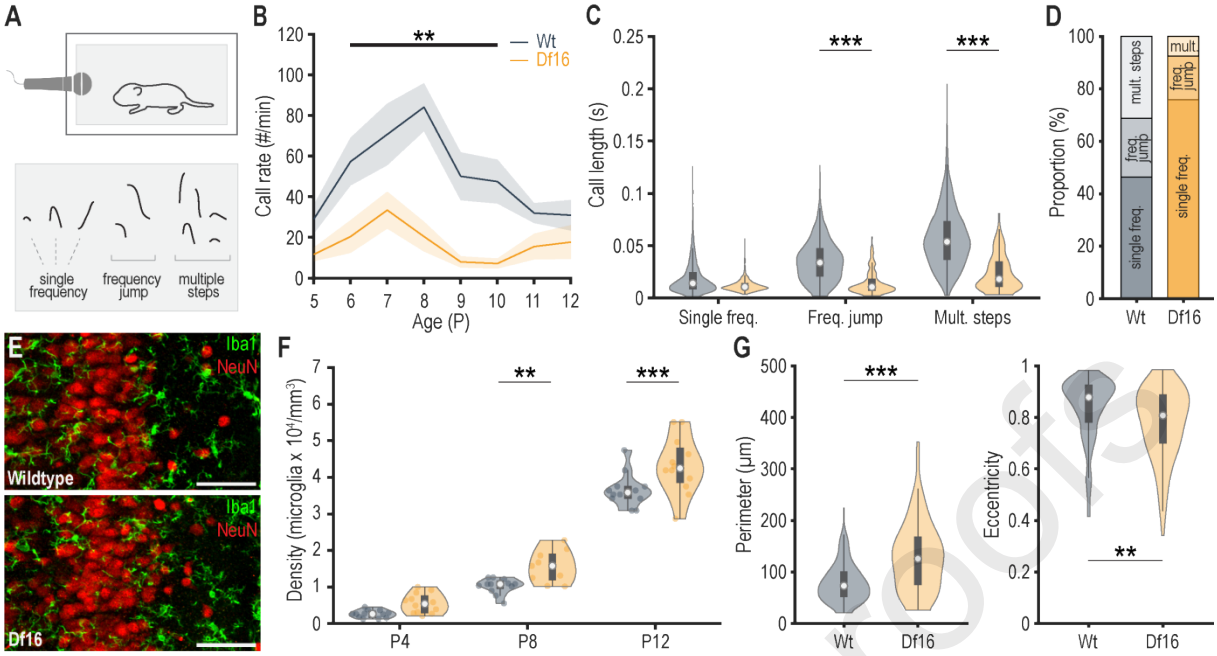

1016

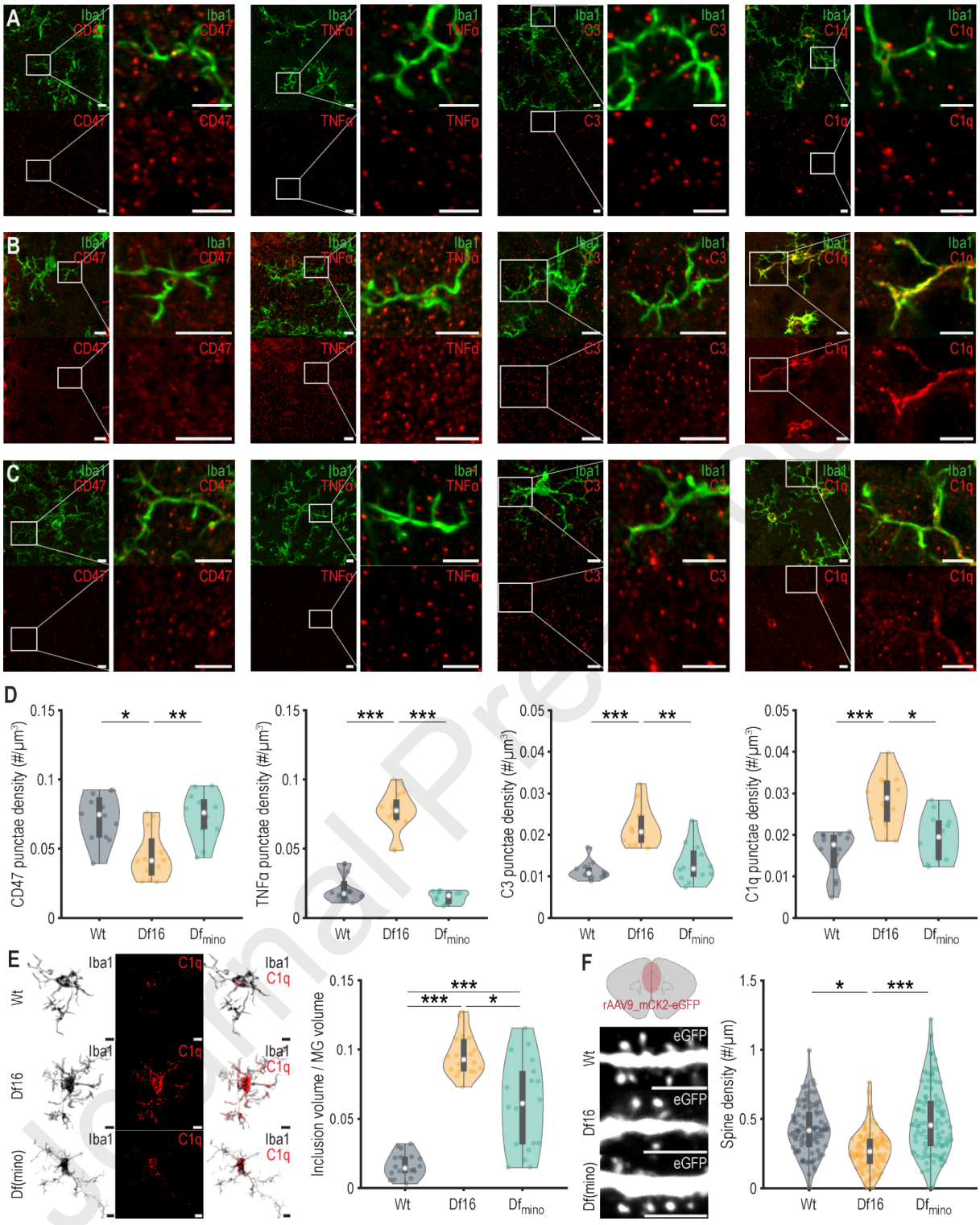

1017

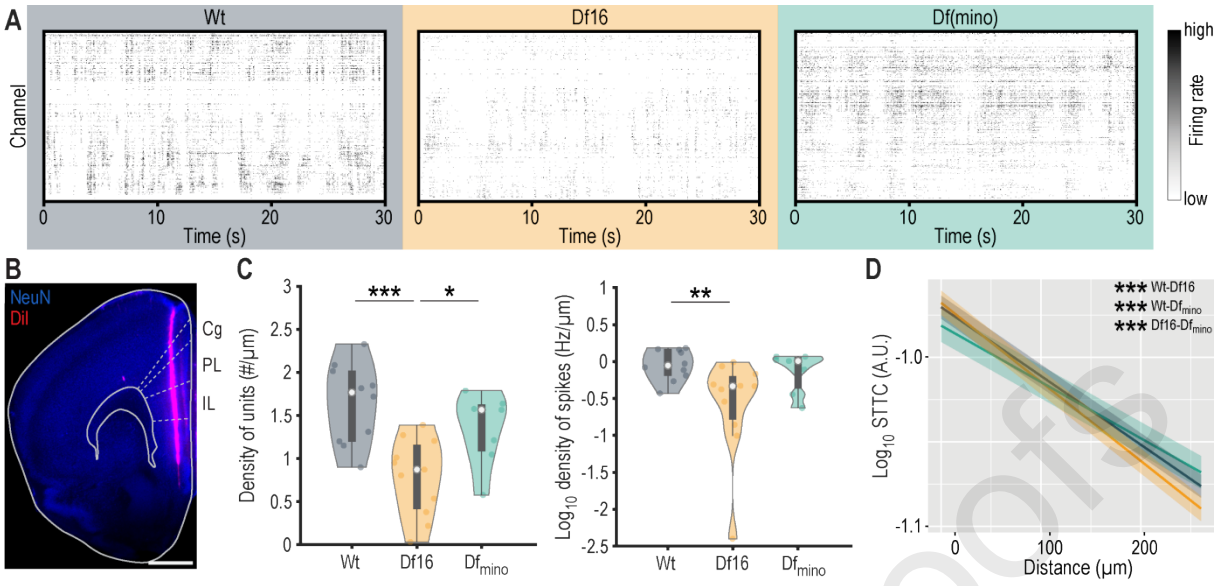

1018

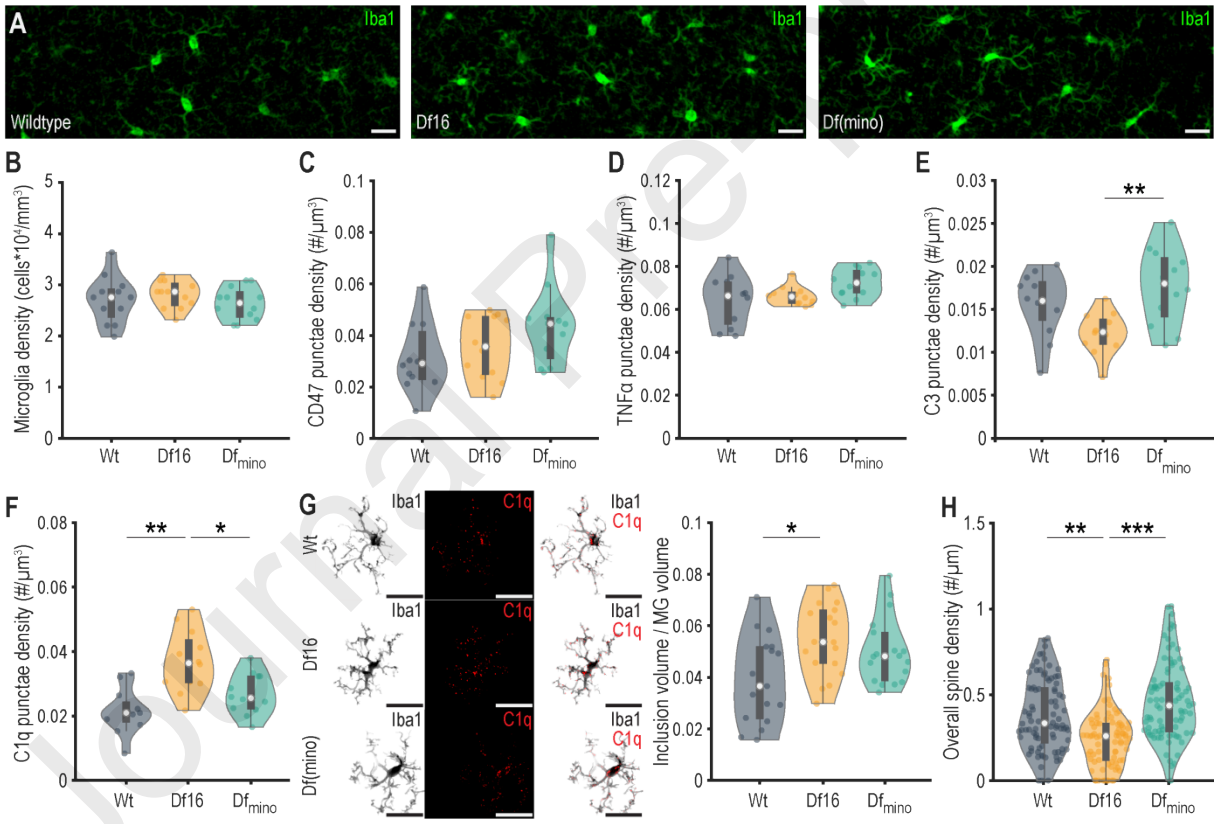

1019

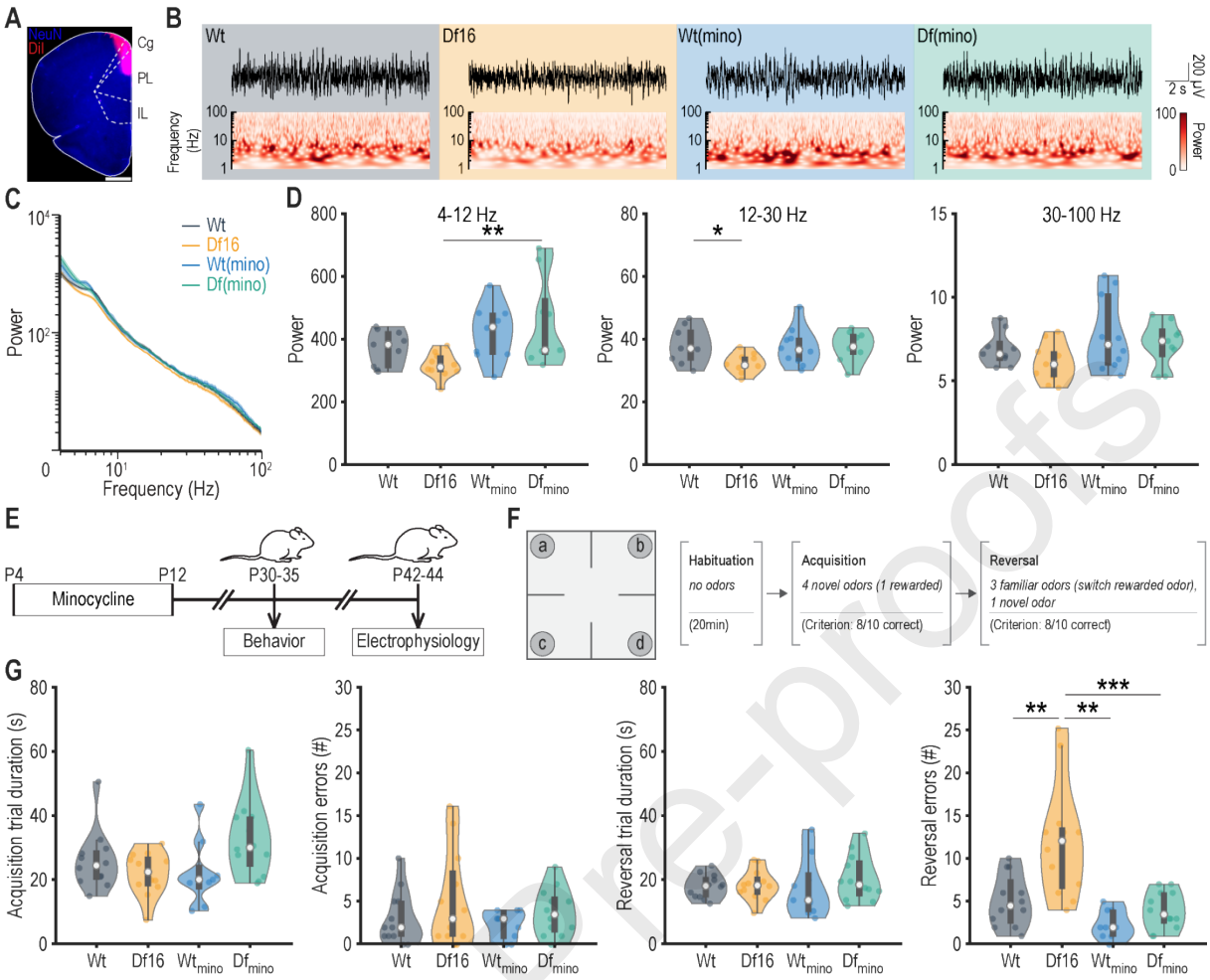

1020